Helium Measurements of Pore-Fluids obtained from SAFOD drillcore

Ali, S. (1,2,5*), Stute, M. (1,3), Torgersen, T (1,4,6*), Winckler, G. (1,2), Kennedy, B.M. (5)

[1]Lamont-Doherty Earth Observatory, Palisades, NY
[2]Department of Earth and Environmental Sciences, Columbia University, New York, NY
[3]Department of Environmental Science, Barnard College, New York, NY
[4]Department of Marine Sciences, University of Connecticut, Groton, CT
[5]Lawrence-Berkeley National Laboratory, Berkeley, CA
[6]National Science Foundation, Arlington, VA

*Current address

Abstract

^{4}He accumulated in fluids is a well established geochemical tracer used to study crustal fluid dynamics. Direct fluid samples are not always available; therefore, we have adapted a method to extract rare gases from matrix fluids of whole rocks by diffusion. Helium was measured on matrix fluids extracted from sandstones and mudstones recovered during San Andreas Fault Observatory at Depth (SAFOD) drilling. Samples were typically collected as subcores or from drillcore fragments.

Helium was measured 4-6 times on each sample, and indicate a bulk ^{4}He diffusion coefficient of $3.5\pm1.3\times10^{-8}$ cm^2s^{-1} at 21^{o}C, compared to diffusion coefficients of 1.2×10^{-18} cm^2s^{-1} (21^{o}C) to 3.0×10^{-15} cm^2s^{-1} (150^{o}C) in the sands and clays (Solomon et al. 1996). Correcting the diffusion coefficient of $^{4}He_{water}$ for matrix porosity (~3%) and tortuosity (~6-13) produces an effective diffusion coefficient of 1×10^{-8} cm^2s^{-1} (21 ^{o}C) and 1×10^{-7} (120 ^{o}C), effectively isolating matrix pore fluid ^{4}He from the ^{4}He contained in the rock matrix. Model calculations indicate that less than 6% of He initially dissolved in pore fluids was lost during the sampling process. Complete and quantitative extraction of the pore fluids provide minimum in situ porosity values for sandstones 2.8±0.4% (s.d., n=4) and mudstones 3.1±0.8% (s.d., n=4).

I. Introduction

The mechanisms and rates of fluid transport in rock are an important control on a) basic fluid transport in the Earth's crust (Fyfe, 1978; Torgersen, 1989) , b) radioactive waste disposal (i.e. Olanrewaju, 2009) or carbon dioxide storage in deep geological formations (e.g. Orr, 2009 and references therein), and c) understanding fluid processes in fault zones (Sano et al., 1986; Kulongoski et al., 2003; Kulongoski et al., 2005; Kennedy and van Soest, 2007; Suer et al., 2008). Below melting temperatures, fluid flow represents the most common form of chemical transport in the crust (Fyfe, 1978; NRC, 1990), thus pore fluid chemistry and geochemical tracers are essential in constraining sources, sinks and timescales for fluid flow. These processes can be evaluated in situ only on the short- time and space scales. Long timescale quantification of fluid flow typically requires geochemical tracer techniques and collection of in situ fluids. Traditionally, geochemical measurements are performed on fluid-only samples collected from wells or bailers in boreholes. However, direct fluid samples are not always available, may be of poor quality because of contamination or don't provide adequate spatial resolution.

The San Andreas Fault Observatory at Depth (SAFOD) drilling project was undertaken to investigate the physical, chemical and hydrologic processes controlling faulting and earthquake generation within a seismically active, major plate-bounding fault (Zoback, 2006). Geophysical logs from the SAFOD drill hole show several sharp transitions in resistivity across the damage zone (3200-3400 m-MD) (Hickman, 2007), which could be a result of weak and highly fractured rocks and/or changes in pore fluid pressure (Mishina, 2009). To trace the origin and transport of fluids within the San Andreas Fault, we exploit the low natural

abundance, chemical inertness, and distinct isotopic signature of noble gases to provide insight into source and timescales of fluids in the different crustal environments that comprise the SAF. For the SAFOD drilling project, the drilling plan did not (generally) expect enough fluid inflow throughout scheduled drilling phases to enable fluid-only sampling. Furthermore, slow flow and drilling costs suggested that devoting time to allow the drill hole to infill with fluids might have been prohibitively expensive. Within these constraints, we used whole rock samples to collect matrix pore fluid samples from SAFOD solid phase drill cores adapting a methodology pioneered by the Institute for Environmental Physics at the University of Heidelberg, Germany (Osenbrück et al., 1998; Lippmann et al., 2002; Rübel et al., 2002). Upon recovery and suitable containment, the relaxation of the rock (released from e.g. 2km of lithostatic pressure) allowed the matrix pore fluids to be extracted. This paper demonstrates an effective method to extract matrix pore fluids and helium from drill core samples and represents the first attempt to extract pore fluids from altered sedimentary rocks from an actively creeping fault zone undergoing repeated or continuous fluid-rock interaction at 120ºC in situ temperature.

a. Geological Setting: The SAFOD drill site

The SAFOD drill site is located near Parkfield, CA, the fault, separates the North American Plate in the northeast from the Pacific Plate in the southwest. SAFOD phases 1 and 2 (conducted in 2004 and 2005, respectively) included drilling the main hole (MH) to a vertical depth of ~1.7 km followed by an angled descent intersecting the trace of the San Andreas Fault at ~2.7 km vertical depth, or ~4 km measured depth (MD) along the borehole. SAFOD MH was drilled in 2004 to a depth of 3051 m (Phase 1) and deepened to 3987 m in 2005 (Phase 2). Spot cores were obtained from1462-1469m, 3056-3067m MD during Phase 1 and from 3990-

3993 m MD during Phase 2. Phase 3 recovered cores from 3141-3153 m MD, 3186-3198 m MD, 3294-3313 m MD in 2007. Figure 1 highlights the drillhole lithology as well as our sample depths in context of geophysical log data. The bulk mineralogy of the SAFOD drill cuttings show an arkosic rock sequence from 1920-2550 m, separated by a clay-rich zone at 2550-2680 m MD and a fine-grained sequence at 2680-3150 m MD. A lithologic change occurs at ~ 3150 m MD, where arenites are replaced by fine-grained siltstone and shale fragments. The section at 3150-3550 m MD is characterized by a fine-grained quartz-feldspar rich mudrock (siltstone and shales) with interbedded sandstones (Bradbury et al., 2007). The relative locations of depths corresponding to the Pacific Plate, SAF damage zone, and the North American Plate are based on geophysical logs from Zoback et al. (in press).

Other studies have been performed on fluids collected in the study area (Kennedy et al., 1997). Fluid samples from springs, seeps and wells associated with the San Andreas Fault have been analyzed to investigate whether fluid movements play a role in the San Andreas Fault dynamics (Kennedy et al., 1997). SAFOD drilling hiatuses in 2004 and 2005 allowed some direct fluid sampling but the inflow zones (depths) were not well constrained and the number of samples obtained does not allow adequate examination of SAF fluid processes (Thordsen et al., 2005).

Erzinger et al. (2004) and Wiersberg and Erzinger (2007) applied real-time mud gas analyses during drilling, a well known monitoring technique from oil and gas drilling, to gain information on crustal fluids and gases encountered in the SAFOD hole. The mud logging method takes advantage of gas release via mechanical crushing of rocks during drilling and provides initial qualitative

information about the gas content of the drilled section. However, it does not provide a (high resolution) quantitative measure of fluid composition (e.g. concentration of dissolved gases) (Erzinger et al., 2004).

To fill this gap in knowledge about the fluid composition in the SAFOD fault zone, this project collected 2.54cm subcore rock samples from the primary project drillcore recovered and extracted matrix pore fluids contained within the subcore samples. In this manner, we were able to collect a suite of samples across the seismogenic zone, measure noble gases and to define fault zone processes with gradients in helium isotope concentration. Here we describe in detail the methodology for this sampling and extraction procedure and use the method to detail the tortuosity of the rocks sampled as controls on porefluid transport.

II. Methods

a. Onsite sampling

We adapted a methodology pioneered by the Institute for Environmental Physics at the University of Heidelberg, Germany (Osenbrück, 1996; Lippmann, 1997; Osenbrück et al., 1998; Rübel, 1999; Rübel et al., 2002). SAFOD scientific drillcores (~10 cm diameter) in Aluminum (Al) liners were recovered to the surface as soon as possible after coring. The ends of the core segments were then subcored using a 2.54cm hollow stem rock drill with de-ionized water (DI) as drilling fluid. This procedure avoids sampling material on the outside of the core that may have degassed already (see Fig 2.9 and Fig. 2.10 of Osenbrück 1996) or has been contaminated with drilling fluids during recovery of core in the borehole. On other occasions, similarly-sized loose rock fragments were obtained from inside the core barrel where sub coring was not possible due to the brittle nature of rock type (i.e. in siltstone or

shale). See Fig. 1 for sample depths. The subcore sample was immediately dried with a paper towel and placed into a stainless steel high vacuum container and sealed (figure 2a). The air inside the container was pumped with a rotary pump for 30 seconds and the container was then filled with research grade (Nitrogen) N_2 to a pressure of about100 mbar. The container was again evacuated for 30 seconds and filled with N_2 to 100mbars. Finally the sample container was evacuated for 45 seconds before it was closed off. The sample was then stored at room or elevated temperature (120^{o}C, in situ temperature, see below) to allow for quantitative dewatering, head space degassing and collection of pore fluid gases. The drill core samples analyzed for this study are marked in Fig. 1 and summarized in Table 1.

b. Tests of field sampling procedure

In order to quantify the amount of fluid lost during the drying, pumping and purging process in the field (discussed in section IIa), we replicated the field procedure on re-saturated shaley siltstone and sandstone samples in the lab. Each rock sample was dried in an oven at 120^{o}C to constant weight, and was submerged in (Carbon dioxide gas) pCO_2 ~ 1000 mbar for two days to replace air within the sample pore spaces and fractures. Then the sample was placed in degassed DI water for two days to re-saturate all accessible pore spaces and fractures before it underwent the same evacuation process as in the field procedure. The sample weight was measured before and after the evacuation process to determine the amount of pore fluid lost during the sampling process in the field. Results are listed in Table 2. Then the sample was dried again at 120°C to constant weight in the oven. The mass of DI water

taken up during re-saturation (re-saturated, wet weight – dry weight) allows us to calculate the porosity ($porosity_2$, listed in Table 2) of the sample at low pressure (i.e. 1 bar compared to lithospheric pressure at depths).

c) Noble gas isotopic analyses

Samples were secured in specially designed soft plastic storage boxes as checked luggage on airplanes. Upon arrival at Lamont Doherty Earth Observatory (LDEO), we applied two different storage schemes to the samples. Two sample containers were held at room temperature for 985 days and were measured six and seven times until the matrix porefluids were completely degassed. Subsequent samples were stored in an oven at in-situ temperature of 120^{o}C (Williams et al., 2004) after the first or second isotope analyses to speed the gas release from the matrix pore fluids.

The full suite of noble gas isotopes (^{3,4}He, $^{20, 21, 22}$Ne, $^{36, 38, 40}$Ar, ^{84,86}Kr, and $^{129,131, 132, 134, 136}$Xe) were determined mass spectrometrically using the LDEO facilities and standard procedures (e.g. Stute et al., 1995). Briefly, gases were extracted from the sampling container after the rock had relaxed over various time periods. . The gas from the sample container was transferred for 30 min through a capillary and a stainless steel trap at ethanol-dry-ice temperature and a 3Å molecular sieve trap at room temperature into an expansion volume (1000cc) by using water vapor from the sample as a carrier gas. A known fraction of dry gas was split off and chemically active gases were removed in a Ti/Zr getter at 800^{o}C. The remaining noble gases were then transferred onto a trap filled with activated charcoal at 13K. After quantitative adsorption, the individual gases were desorbed from the charcoal by stepwise heating and (after exposure to additional getters) transferred into a static sector field mass spectrometer with extended geometry (MAP

215-50, Mass Analyzer Products, Manchester). ^{3}He was measured by pulse counting on an electron multiplier, all the other isotopes were analyzed on a Faraday cup. The overall procedure was calibrated by measuring known quantities of atmospheric air. The precision of isotope ratio determinations are ~2% for $^{3}He/^{4}He$ ratios. The reproducibility of abundance measurements was estimated from air standard measurements to be 2% for He and Ne.

d) Modeling methods

Diffusion coefficients were determined by fitting the cumulative He concentrations with simple analytical and numerical solutions of the diffusion equation for spherical or cylindrical shapes (Crank, 1975). Samples experiencing two different temperatures over time require a numerical solution. For numerical solutions of the diffusion equation, we used the rock sample's actual surface geometry as the diffusion boundary. The sample geometry was determined by a 3D scan via a portable Minolta Vivid 910 laser surface scanner (courtesy of W. Harcourt-Smith, American Museum of Natural History, NY). As in the analytical solutions, the initial concentration was assumed to be a uniform value and the boundary concentration to zero. The sample geometry was discretized with a 3D finite difference grid with a typical grid box size of 42 mm^3 ($(3.5 \text{ to } 4.0mm)^3$ grid over a 25mm diameter rock sample). The diffusion equation was solved with a simple forward finite difference numerical scheme (Bear and Verruijt, 1987).

e) Porosity determination

During each noble gas analysis, the sample water released by the relaxed rock was used as a carrier of gases contained in the container headspace and collected in a dry ice cooled trap. After completion of each extraction (30min), the condensed water vapor

was transferred into a removable water trap cooled to liquid nitrogen temperature and quantified by differential weighing. Following the final extraction, the sample container was vented and each rock subcore sample was weighed immediately before being baked at 120^{o}C in an oven. Each sample's weight was monitored over three days until the weight stayed constant indicating that all mobile water had been removed from the rock sample. The cumulative water content for each sample was determined by adding the amount of transferred water vapor from the sum of extractions for isotopic analyses and the remaining water removed during the bake-out in the oven, as determined by differential weighing of the sample before and after baking. The total water content is representative of the volume of void space in our rock samples. The bulk volume of sample was determined by measuring the displacement of DI water of the samples wrapped in a thin layer of adhesive plastic to avoid filling pore spaces with DI-water. The combination of measurements allows for the determination of bulk density and water content (porosity$_1$) of the samples (see Table 2). The total water content of each sample determined by this process is also used to calculate total helium concentration in the total fluid (i.e. cubic centimeters of helium at standard temperature and pressure per gram of water, ccSTP He/g water).

III. Results

a. Sampling procedure

There are two potential sources of helium contamination that can alter the helium isotope ratios. First, the sampling process in the field required research grade (RG) nitrogen gas to flush out atmospheric gases from the sample container headspace. Our helium blank contribution from the RG nitrogen gas used in the field was less than 0.01 %. The second potential source of helium

contamination is residuals of air in the containers during sampling which was estimated from other noble gases and air-like ratios. Most of the air contamination is based on Ar, Kr and Xe values, all of which are also likely naturally present in the pore fluids and thus this estimate suggests a maximum helium contribution of less than 3% from air during the sampling process. Most samples have less than 1% air contribution to helium as listed in Table 1. TW4 is the only sample with a considerably higher air contribution (2.91%). ^{20}Ne concentrations were used to check for possible degassing of the pore fluids during the sampling process. Pore fluid ^{20}Ne concentrations ($2.6x10^{-7} \pm 1.7x10^{-7}$ (s.d., n=8) ccSTP/g) are consistent with average air saturated Ne values in fresh water and sea water ($1.4x10^{-7}$ to $2.2\ x10^{-7}$ccSTP/g summarized by Kipfer et al. (Kipfer et al., 2002) suggesting that pore fluids extracted from samples with 2.5 cm radius or similar thickness have not degassed during the sampling procedure.

b. Isotope analysis

The reconstructed total helium isotope ratios in matrix pore fluids recovered are 0.373Ra ± 0.006 (s.d., n = 4) from the Pacific Plate and 0.945Ra ± 0.007 (s.d., n = 4) from the North American Plate ($Ra=1.384x10^{-6}$), see Table 1. Figures 3 and 4 show the cumulative ^{4}He concentration as a function of time, using the total extractable water content and cumulative ^{4}He removed over time. The sample always held at room temperature (Figure 3) took more than 900 days for complete degassing, while the sample stored at 120ºC (in situ temperature; Fig. 4) reached complete degassing in less than 400 days. Helium isotope ratios of each measurement are used as an additional degassing indicator. The last three helium concentration measurements in Fig. 4 are two orders of magnitude lower than previous analyses of the same sample and contribute less than 1% to the cumulative helium concentration. The higher

helium isotope ratios observed for the corresponding measurements (marked by 'x' in Fig. 4) are due to atmospheric helium accumulation in the sample container through tiny leaks, corresponding to less than 3% of individual measurements and less than 0.01% of the cumulative helium concentration.

c. Helium diffusion coefficients

Cumulative ^{4}He concentrations as a function of time are used to determine the effective helium diffusion coefficient in the pore fluid matrix within the rock sample. Figures 5 and 6 represent normalized cumulative helium concentration as a function of time in days for samples held at room temperature for over 900 days. The following solutions (Crank 1975) are used to determine analytical solutions of the diffusion coefficients. The solution assumes a uniform initial concentrations of He in the rock sample and a C=0 boundary condition for a spherical (equation 1) and infinite cylindrical geometry (equation 2) of the samples.

$$\frac{M_t}{M_\infty} = 1 - 6\sum_{n=1}^{\infty} \frac{1}{n^2} \exp\left(\frac{-D^2 n^2 \pi^2 t}{r^2}\right) \quad (1)$$

$$\frac{M_t}{M_\infty} = 1 - \sum_{n=1}^{\infty} \frac{4}{r^2 \alpha_n^2} \exp\left(-D\alpha_n{}^2 t\right) \quad (2)$$

where M_t is the summed quantity of diffusing substance which has left the object at time t, M_∞ is the total quantity of substance diffused out of the body after infinite time, D is the bulk diffusion coefficient, r is the sample radius, and α_n are the roots of Bessel function of the first kind of order zero.

The solutions to equations 1 and 2 are also plotted in figure 5. The dashed red and the dotted green lines represent the solutions to equations 1 (spherical boundary, D_1(sphere) = 3.5±1.3 x 10^{-8} cm^2s^{-1}) and equation 2 (cylindrical boundary, D_2(cylinder)=1.5±1.3 x10^{-8} cm^2s^{-1}), respectively. The gray region represents the uncertainty in diffusion coefficients in equation 1 based on the data fit.

Numerical results represented by solid lines in figure 6 correspond to diffusion coefficients of D_4= 6.0x10^{-8} ± 2.0x10^{-8} cm^2s^{-1} (upper limit) and D_3=3.0x10^{-8} ± 1.0x10^{-8} cm^2s^{-1}(best fit).

For samples held at room temperature for 225 days and then held at 120ºC for over 700 days, the normalized cumulative helium concentration versus time is shown in Fig. 6. Due to the change in storage temperature, which we cannot take into account in the analytical solution, we need to rely on the numerical solutions to determine diffusion rates. As shown in Fig.6, the numerical solutions indicate a diffusion coefficient of 1.5x10^{-7} cm^2s^{-1} at 120ºC, a five to ten fold increase compared to diffusion rates at room temperature.

d. Porosity and density determinations

. Table 2 lists density and porosity data for all samples of this study. Our method allows quantitative determination of the pore fluid mass present in the sample at depths, thus enabling us to calculate the minimum porosity (listed as $porosity_1$ in table 2) of each individual sample because some void space could be unsaturated and some water could be lost by towel drying and pumping of the drill core subsample. Based on our re-saturation experiments in the lab (listed in Table 2), towel drying of each sample followed by

evacuation and flushing process in individual sample vacuum containers led to water loss of up to 4.6% in sandstone (Pacific Plate) samples and up to 9% in siltstone (North American Plate) samples.

We observe average porosity$_1$ (based on mass of pore water at depth) values of 2.8±0.4 % (s.d., n=4) and average bulk density values of 2.1±0.3 gmL^{-1} s.d., n=4) in the samples from the Pacific Plate. The North American Plate samples have similar average porosity$_1$ values of 3.1±0.8% (s.d., n=4) and average bulk density of 2.1±0.2 gmL^{-1} (s.d., n=4). One shale sample from ~3400 m (MD) has a porosity$_1$of 6.1%, but this sample was obtained from the core catcher and shows obvious drilling marks. We cannot be sure of the original sample depth and the amount of time it was exposed in the borehole and remove this sample from further discussion.

The re-saturation experiment also provides a measure of porosity of each sample under ambient pressure of 1 bar, which are also listed in table 2 as porosity$_2$ (see section IIIc for definition). Porosity$_2$ values (6.6 ± 1.6 % (1 s.d.) for sandstones from the Pacific Plate, and 5.8 ± 2.8 % (1 s.d.) for North American siltstones) are also indistinguishable within error for samples from the North American and Pacific Plates, but they are consistently higher than porosity$_1$ values due to newly formed fractures during drilling and retrieval of the drill core to much lower pressures.

IV. Discussion

a. Sampling procedure

This procedure was pioneered in Heidelberg by Osenbrück (1996). The Heidelberg study used larger sample size and 70 seconds of pumping (compared to 30-45 seconds of pumping and purging with N_2 used in this study) to evacuate each sample container before sealing the sample. They observed complete degassing of noble gases within one month, which translated into 20-30 % loss of noble gases during the sampling procedure. Given the calculated diffusion coefficients described in section III-c and assuming He loss due to diffusion at room temperature, we estimate a 4 to 6% loss of helium during sampling (this study) compared to 20-30 % loss reported by Osenbrück (1996).

Laboratory tests showed that repeated pumping and purging with research grade N_2 (this study) is effective in removing >99.99% of the air (based on Ar, Kr and Xe analysis of each extraction) within the container (replaced with high purity N_2 at low pressure). 0.01% air contamination would affect the helium isotope ratio (R/Ra) by less than 1%, which is within the analytical uncertainty and therefore has no impact on the helium isotope data interpretation of these samples.

b. Helium isotope concentrations and ratios

Table l lists helium isotope ratios and helium abundance data derived by three different methods applied to samples from similar depths of the SAFOD drill hole. The pore fluid diffusion method is described in this study. The mudgas (Wiersberg and Erzinger 2007) samples are released from mechanical crushing of rocks during drilling and have relatively larger error bars due to atmospheric contamination. Lawrence Berkeley National Laboratory (LBNL) data (Table 1) are derived from fluid samples collected (4-6 months) after drilling and during drilling hiatuses. The bore hole walls were cased with cement to a depth of 3050 m (MD) before fluid was

allowed to collect in the depth interval between 3050 m to 3065 m (MD) and subsequently sampled in 2005 (samples 05WPT1, 05WPT2, and SAF206 retrieved from 3051-3064 m MD). After the bore hole was deepened and cased to a measured depth of 3990 m (MD), fluids accumulated for several months before further fluid sampling in 2006 (samples SAF205 and SAF202 retrieved from 3261m and 3726m MD, see table 1). Under these conditions, the fluid is expected to fill the well from the bottom (uncased section) of the borehole.

Matrix pore fluid helium concentrations are constant on both plates (Pacific Plate: $1.9\pm0.5 \times 10^{-5}$ ccSTPg^{-1} (s.d., n=4), North American Plate: $1.4\pm0.1 \times 10^{-5}$ ccSTPg^{-1} (s.d., n=4)). The helium concentrations of fluid samples collected from open intervals of the bore hole was calculated from F(^{4}He) and F(^{40}Ar) data (measured at LBNL; F(N_g)=[N_g]/[^{36}Ar]) and Ar concentration data obtained from individual fluid sample splits (listed in Table 1). The direct fluid sample concentrations also yield similar average helium concentrations on both plates (Pacific Plate: $5\pm2 \times 10^{-5}$ ccSTPg^{-1} (1 s.d., n=3), North American Plate: $6\pm3 \times 10^{-5}$ ccSTPg^{-1} (1 s.d., n=2)) although they are at least two times larger than the matrix pore fluid helium content (see Fig. 7a). If the ^{20}Ne concentration data are a good indicator of the robustness of this (pore fluid extraction) method, then the higher ^{4}He abundance in well fluids could likely be due to fracture fluids tapping into a different (older) reservoir compared to local fluids contained in matrix pore fluids. However, the consistent ^{3}He/^{4}He ratios observed in well fluids and pore fluids would suggest that the fluids contained in fractures and pore spaces are in equilibrium. However, we do not have enough information to further evaluate this possibility.

In general, gas abundances in well fluids are measured from the sample container head space on a gas chromatograph (GC). The helium concentrations in the well fluid samples recovered during SAFOD drilling project were very small (very close to the GC detection limit). The well fluid [He] data listed in table 1 are calculated based on ^{40}Ar abundance data from the sample container head space measured on a GC (United States Geological Survey, Menlo Park, CA) and $^{4}He/^{36}Ar$ and $^{40}Ar/^{36}Ar$ ratios from split fluid samples measured on a mass spectrometer (at Lawrence Berkeley National Laboratory, Berkeley, CA) (Thordsen et al. 2005) . Thus, we are completely confident in the well fluid helium abundance data presented in table 1.

However, the pore fluid helium isotope ratios (Fig. 7b) suggest two distinct sources of fluids in the Pacific Plate (R/Ra=0.373±0.006 (1 s.d., n=4)) and the North American Plate (R/Ra=0.945±0.007 (n=4)). These ratios are remarkably consistent with direct fluid data (LBNL data, table 1) as well as mud gas data (Wiersberg and Erzinger 2007), suggesting isotopic equilibrium on each side of the SAF. However the pore fluid data are three times more precise as indicated by the error bars in Fig. 7b compared to mud gas samples associated with the SAF (samples labeled as Wiersberg et al., table 1).

c. Helium diffusivity

Helium diffusion coefficients calculated with cylindrical and spherical boundary conditions are the same within one sigma error. As seen in Fig. 5, the numerical model (for $D_3=3x10^{-8} \pm 1.0x10^{-8}$ cm^2s^{-1} and $D_4=6x10^{-8} \pm 2.0x10^{-8}$ cm^2s^{-1}) mimics the analytical solutions ($D_{1sphere}$ and $D_{2cylinder}$) closely and provides the same diffusion coefficients (within error) for samples held at room temperature. D_4 in Fig. 5 is likely higher due to newly formed fractures in each sample under low pressure that provides a connected

path for fluid flow out of the rock matrix. We observe an approximate five- to ten-fold increase in the diffusion coefficient of helium at 120ºC relative to 21ºC ($1.1x10^{-8}$ cm^2s^{-1} at 21°C and $1.5x10^{-7}$ cm^2s^{-1} at 120°C) allowing for faster sample degassing. Helium diffusion coefficients measured in the solid phase of sands and clays are 1.2×10^{-18} cm^2s^{-1} at 21°C and $3.0x10^{-15}$ cm^2s^{-1} at 150°C (Solomon et al., 1996). Diffusion coefficients calculated in this study are several orders of magnitude larger and characterize helium derived from matrix pore fluids. Fig. 5 also shows the theoretical cumulative helium concentration over 1000 days for an estimate of a solid phase diffusivity of $D_s=1.0x10^{-15}$ cm^2s^{-1} in comparison to SAF4 and SAF5 data, as well as analytical and numerical diffusion curves. The stark contrast between our data and the solid phase scenario illustrates that noble gases collected in this fashion represent matrix pore fluid noble gases and not solid phase noble gases.

d. Porosity and density

In order to constrain helium concentrations, this method relies on accurate determination of matrix pore water mass, which is accomplished by quantitative extraction of matrix pore fluids from each rock sample. The extracted water vapor is released from connected pore spaces filled with fluid and thus corresponds to the minimum porosity of each sample. Porosity and density data of each sample are compared to geophysical logs obtained from the same depth in table 2. Density results of individual hand samples (Pacific Plate: 2.1 ± 0.3 gmL^{-1} (s.d., n=4), North American Plate: 2.1 ± 0.2 gmL^{-1} (s.d., n=4)) are consistent to neutron density logs (Pacific Plate: 1.9 ± 0.4 gmL^{-1} (s.d., n=4)). The minimum in situ porosity ($porosity_1$) values (Pacific Plate: 2.8 ± 0.4 % (s.d., n=4) and

North American Plate: 3.1±0.8 % (s.d., n=4)) obtained in this study are lower than the field normalized compensated neutron porosity log (SAFOD Main Hole downhole logging data phase 2 (2005), 2812-3043m (DOI: 10.1594/GFZ.SDDB.1126); 2975-3387m (DOI: 10.1594/GFZ.SDDB.1127); 3387-3799m (DOI: 10.1594/GFZ.SDDB.1128) by at least a factor of two. $Porosity_2$ values listed in Table 2 and derived from the re-saturated weight in individual rock samples with DI water are much closer to the geophysical logging porosity values. However, the higher values in $porosity_2$ are due to a combination of complete saturation of void spaces within the rock matrix with DI water and newly formed fractures due to lower pressure that enhance the void space in the rock matrix allowing more water to be absorbed by each rock. Thus far, the porosity values ($porosity_1$ in Table 2) obtained from this study are a minimum representation of porosity at depth. Based on the density and porosity data found in this study, individual sandstone and siltstone samples are indistinguishable from each other (see Table 2 and figure 1).

e. Tortuosity

Rock samples in an active fault zone (i.e. the San Andreas Fault) are altered by multiple fracture formation and fluid-rock interaction events that result into continuous evolution of connected pore spaces and fractures thereby affecting tortuosity in the rock matrix. A comprehensive list of theoretically derived tortuosity values, for a variety of unconsolidated sediments with porosities ranging from 30-100%, is summarized by Boudreau (1997). Tortuosity in low porosity, consolidated rocks is not well constrained. Diffusion coefficients of helium in pure water are $D_g=6.9x10^{-5}$ cm^2s^{-1} at 21ºC (Jahne et al., 1987) and $17.8x10^{-5}$ cm^2s^{-1} at 120ºC (Solomon et al., 1996). However, the observed diffusion coefficients of gases in pore fluids are also influenced by the porosity and

tortuosity. Since this method provides porosity (p) and effective diffusivity (D_e, $1x10^{-8}$ cm^2s^{-1} to $6x10^{-8}$ cm^2s^{-1}), and diffusion coefficients of helium (D_g) in water is known, we use the relationship described in equation 3 (Van Brakel, 1975) to determine tortuosity (τ) for samples with low porosity values of ~3%.

$$D_e = \frac{D_g}{\tau^2} p \qquad (3)$$

Using this method, we obtained tortuosity values of 6 to 13, which are consistent with studies on shales (Kastube et al., 1991) and clay-enriched sand and siltstones (Salem, 2005).

V. Conclusions:

The method presented in this paper is effective in completely extracting pore fluid content of sedimentary rocks. It provides a viable measure of dissolved gases in matrix pore fluids consistent with established mud gas and direct-sampling fluid methods and allows for both noble gas abundance and isotope analyses. The field procedure minimizes noble gas loss by limiting sampling time to 2-5 hours after core recovery. This procedure, however, requires quick onsite decision making about sampling requirements and sampling frequency, which may not be desirable or possible at all times. Because the entire pore fluid helium content and the complete pore fluid mass were determined, additional properties such as in situ porosity (~3%) and tortousity (6-13) were also calculated.

VI. Acknowledgements

We are grateful to the SAFOD PIs Bill Elsworth, Steven Hickman, and Mark Zoback for their help and support before, during, and after the field experiment; Jim Thorsdsen (USGS) for fluid sampling and William Evans (USGS) for Ar analysis of the fluid samples. We would like to extend special thanks to W. Harcourt-Smith (American Museum of Natural History, NY) for the use of 3D laser scanner and to Linda Baker (LDEO) for assistance with analytical measurements of pore fluids. This work was supported by the US National Science Foundation under grants EAR 04-54514 and 07-45965. This work was partially funded by the Director, Office of Science, Office of Basic Energy Sciences, Chemical Sciences, Geosciences and Bioscience Program of the U. S. Department of Energy under Contract No. DE-AC02-05CH11231. This is LDEO contribution.

VII. References:

Bear, J., Verruijt, A. (1987). Modeling groundwater flow and pollution: with computer programs for sample cases. Dordrecht, Holland, D. Reidel Publishing Company.

Boudreau, B. P. (1997). Diagenetic Models and Their Implementation Modeling Transport and Reactions in Aquatic Sediments. Berlin, Springer.

Bradbury, K. K., Barton, D. C., Solum, J. G., Draper, S. D., Evans, J. P. (2007). "Mineralogic and textural analyses of drill cuttings from the San Andreas Fault Observatory at Depth (SAFOD) boreholes: Initial interpretations of fault zone composition and constraints on geologic models." Geosphere 3(5): 299-318.

Crank, J. (1975). The mathematics of diffusion. Oxford, Oxford University Press.

Erzinger, J., T. Wiersberg, Dahms, E. (2004). "Real-time mud gas logging during drilling of the SAFOD Pilot Hole in Parkfield, CA." Geophysical Research Letters 31(15).

Fyfe, W. S., Price, N.J., Thompson, A.B. (1978). Fluids in the Earth's Crust. New York, Elsevier Scientific Publishing Company.

Hickman, S., M. Zoback, W. Ellsworth, N. Boness, P. Malin, S. Roecker, and C. Thurber (2007). "Structure and properties of the San Andreas Fault in Central California: Recent Results from the SAFOD experiment." Scientific Drilling(Special Issue No.1): 29-32.

Jahne B, Heinz G, Dietrich, W. (1987). "Measurement of the diffusion-coefficients of sparingly soluble gases in water." Journal of Geophysical Research-Oceans 92(C10): 10767-10776.

Kennedy, B. M., Kharaka, Y. K., Evans, W. C., Ellwood, A., DePaolo, D. J., Thordsen, J., Ambats, G., Mariner, R. H (1997). "Mantle fluids in the San Andreas fault system, California." Science 278(5341): 1278-1281.

Kennedy, B. M. and M. C. van Soest (2007). "Flow of mantle fluids through the ductile lower crust: Helium isotope trends." Science 318(5855): 1433-1436.

Kipfer, R., Aeschbach-Hertig, W., Peeters, F., Stute, M. (2002). Noble gases in lakes and ground waters. Noble Gases in Geochemistry and Cosmochemistry. D. Porcelli, C. J. Ballentine and R. Wieler. Washington, Mineralogical Soc America. 47: 615-700.

Kulongoski, J. T., D. R. Hilton, Izbicki, J.A. (2003). "Helium isotope studies in the Mojave Desert, California: implications for groundwater chronology and regional seismicity." Chemical Geology 202(1-2): 95-113.

Kulongoski, J. T., D. R. Hilton, , Izbicki, J.A. (2005). "Source and movement of helium in the eastern Morongo groundwater Basin: The influence of regional tectonics on crustal and mantle helium fluxes." Geochimica Et Cosmochimica Acta 69(15): 3857-3872.

Lippmann, J., Rüble, A., Osenbrück, K., Sonntag, C., and Gröning, M. (1997). Dating porewater in rock samples from fresh drilling cores: Depth profiles of stable isotopes, noble gases and chloride in hydraulically impermeable geological formations. . Isotope Techniques in the Study of Environmental Change. Vienna, Proc. Symp., IAEA.

Lippmann, J., Stute M., Torgersen, T., Moser, D.P., Hall, J., Lihung, L., Borcsik, M., Bellamy, R.E.S., Onstott, T.C. (2002). "Dating ultra-deep mine waters with noble gases and Cl-36, Witwatersrand Basin, South Africa." Geochimica Et Cosmochimica Acta 66(15A): A458-A458.

Mishina, M. (2009). "Distribution of crustal fluids in Northeast Japan as inferred from resistivity surveys." Gondwana Research 16(3-4): 563-571.

National Research Council (NRC) (1990). The role of fluids in crustal processes. Washington, D.C., National Academy Press.

Olanrewaju, J. (2009). "Radioactive Waste Management." Water Environment Research 81(10): 1836-1844.

Orr, F. M. (2009). "Onshore Geologic Storage of CO2." Science 325(5948): 1656-1658.

Osenbrück, K. (1996). Alte und Dynamik tiefe Grundwasser: eine neue Methodik zur Analyse der Edelgases im Porenwasser von Gesteinen., University of Heidleberg. PhD: 116.

Osenbrück, K., J. Lippmann, Sonntag, C. (1998). "Dating very old pore waters in impermeable rocks by noble gas isotopes." Geochimica Et Cosmochimica Acta 62(18): 3041-3045.

Rübel, A., Lippmann, J., Sonntag, C. (1999). Noble gases and isotopes from porewater and rocks. . Monte Terri Rock Laboratory-Results of the hydrogeological, geochemical and geotechnical experiments performed in 1996 and 1997. M. Thury, Bossart, P., Geological Reports Swiss National Hydrological and Geological Survey 23: 148-151.

Rübel, A. P., C. Sonntag, Lippman, J., Pearson, F.J., Gautschi, A.A. (2002). "Solute transport in formations of very low permeability: Profiles of stable isotope and dissolved noble gas contents of pore water in the Opalinus Clay, Mont Terri, Switzerland." Geochimica Et Cosmochimica Acta 66(8): 1311-1321.

Salem, H. (2000). “Fluid-Flow Characterization of Porous Media (for the Example of the Jeanne d’Arc Basin Consolidated Reservoirs)”. Energy Sources, Jul2000, Vol. 22 Issue 6, p557-572, 16p,

Sano, Y., Y. Nakamura, Wakita, H., Notsu, K., Kobayashi, Y. (1986). "HE-3/HE-4 ratio anomalies associated with the 1984 western nagano earthquake - possibly induced by a diapiric magma." Journal of Geophysical Research-Solid Earth and Planets 91(B12): 2291-2295.

Solomon, D. K., A. Hunt, Poreda, R.J. (1996). "Source of radiogenic helium 4 in shallow aquifers: Implications for dating young groundwater." Water Resources Research 32(6): 1805-1813.

Stute, M., J. F. Clark, Schlosser, P., Broecker, W.S., Bonani, G. (1995). "a 30,000-yr continental paleotemperature record derived from noble-gases dissolved in groundwater from the san-juan basin, new-mexico." Quaternary Research 43(2): 209-220.

Suer, S., Gulec, N., Mutlu, H., Hilton, D.R., Cifter, C., Sayin, M. (2008). "Geochemical monitoring of geothermal waters (2002-2004) along the North Anatolian Fault Zone, Turkey: Spatial and temporal variations and relationship to seismic activity." Pure and Applied Geophysics 165(1): 17-43.

Thordsen, J.J., Evans, W.C., Kharaka, Y.K., Kennedy, B.M., van Soest, M. (2005). "Chemical and Isotopic Composition of Water and Gases From the SAFOD Wells: Implications to the Dynamics of the San Andreas Fault at Parkfield, California" American Geophysical Union, Fall Meeting 2005, abstract #T23E-08.

Torgersen, T. (1989). "Terrestrial helium degassing fluxes and the atmospheric helium budget - implications with respect to the degassing processes of continental-crust." Chemical Geology 79(1): 1-14

Van Brakel, J., Pore space models for transport phenomena in porous media, Powder Technology, 1975.

Wiersberg, T. and J. Erzinger (2007). "A helium isotope cross-section study through the San Andreas Fault at seismogenic depths." Geochemistry Geophysics Geosystems 8.

Williams, C. F., F. V. Grubb, Galanis, S.P. (2004). "Heat flow in the SAFOD pilot hole and implications for the strength of the San Andreas Fault." Geophysical Research Letters 31(15): 4.

Zoback, M.D. (2006): SAFOD Penetrates the San Andreas Fault. Scientific Drilling, 2(2006):32-33. (doi:10.2204/iodp.sd.2.07.2006)

Zoback, M.D., Ellsworth, W., Hickman, S. (in press). "Scientific drilling into the San Andreas Fault Zone overview and research opportunities." EOS.

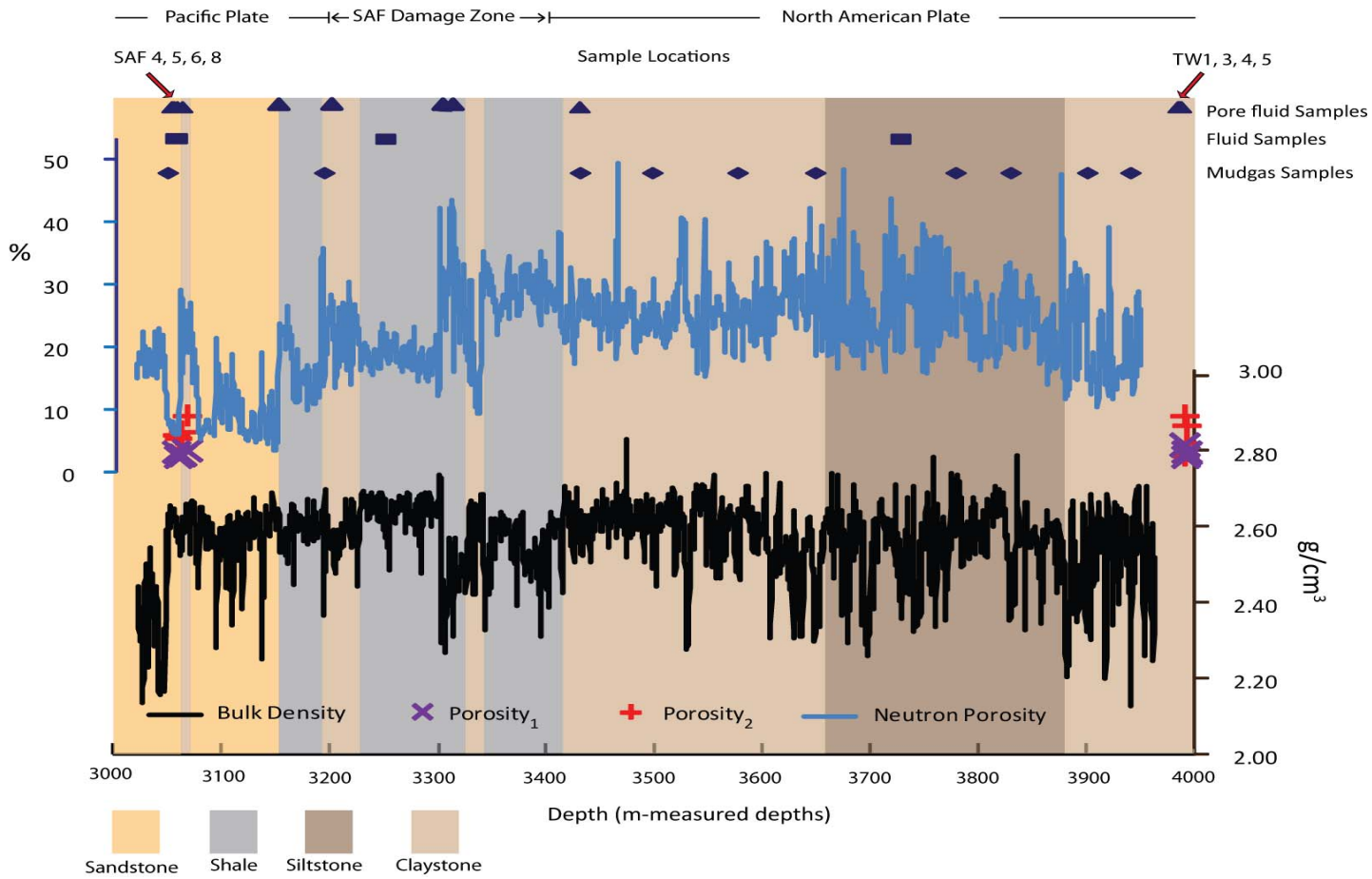

Figure 1: Geophysical log data from SAFOD Phase 2 Highlighted colors correspond to rock type and are based on SAFOD hole drill cuttings as a function of measured depths. Neutron porosity (blue) and bulk density (black) are based on geophysical logs.(DOI: 10.1594/GFZ.SDDB.1126-1128) Sample locations indicated by triangles (matrix pore fluids, this study), squares (fluid samples, this study), and diamonds (mudgas samples, Wiersberg et al.) on top. Porosity$_1$ (purple x) and porosity$_2$ (red +) values obtained from individual samples are also plotted with respect to the % scale. Depths labeled as Pacific Plate, SAF damage zone, and North American Plate are based on geophysical logs by Zoback et al., EOS, in press.

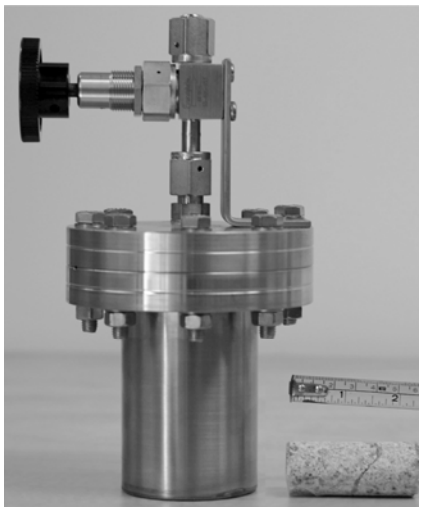

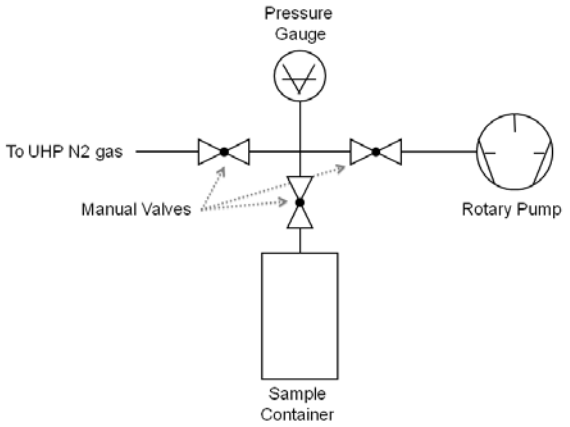

(a) **(b)**

Figure 2: Field sampling apparatus. (a) Stainless steel vacuum sample container next to a subcore sample. (b) Field set-up diagram for evacuating and flushing sample with research grade N_2 before sample is sealed.

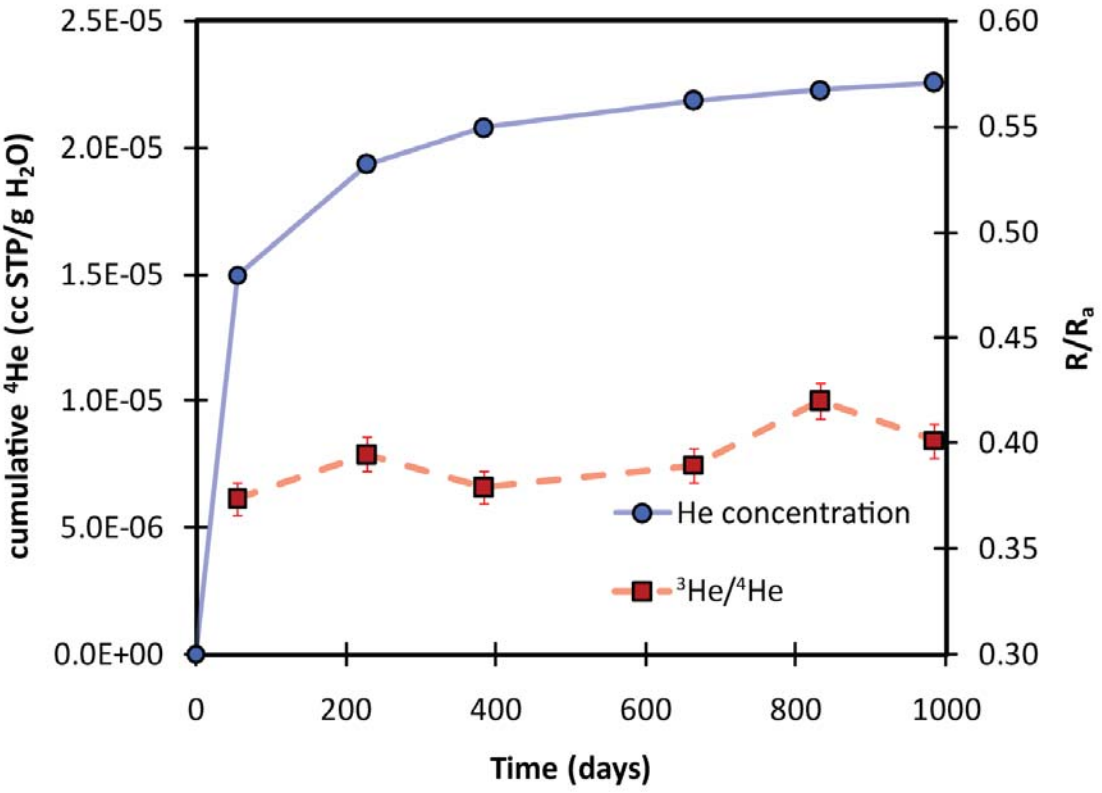

Figure 3: Helium isotope data for SAF 4 (arkosic sandstone, 3059.3-m MD) held at 21°C over six measurements and 1000 days. Blue circles represent cumulative helium concentration in extracted matrix pore water over time, while red squares correspond to $^3He/^4He$ isotope ratio (ratios, R are normalized to air, Ra =$1.384x10^{-6}$) plotted on the right axis. 1σ error bars for helium concentrations are smaller than the size of the blue symbols.

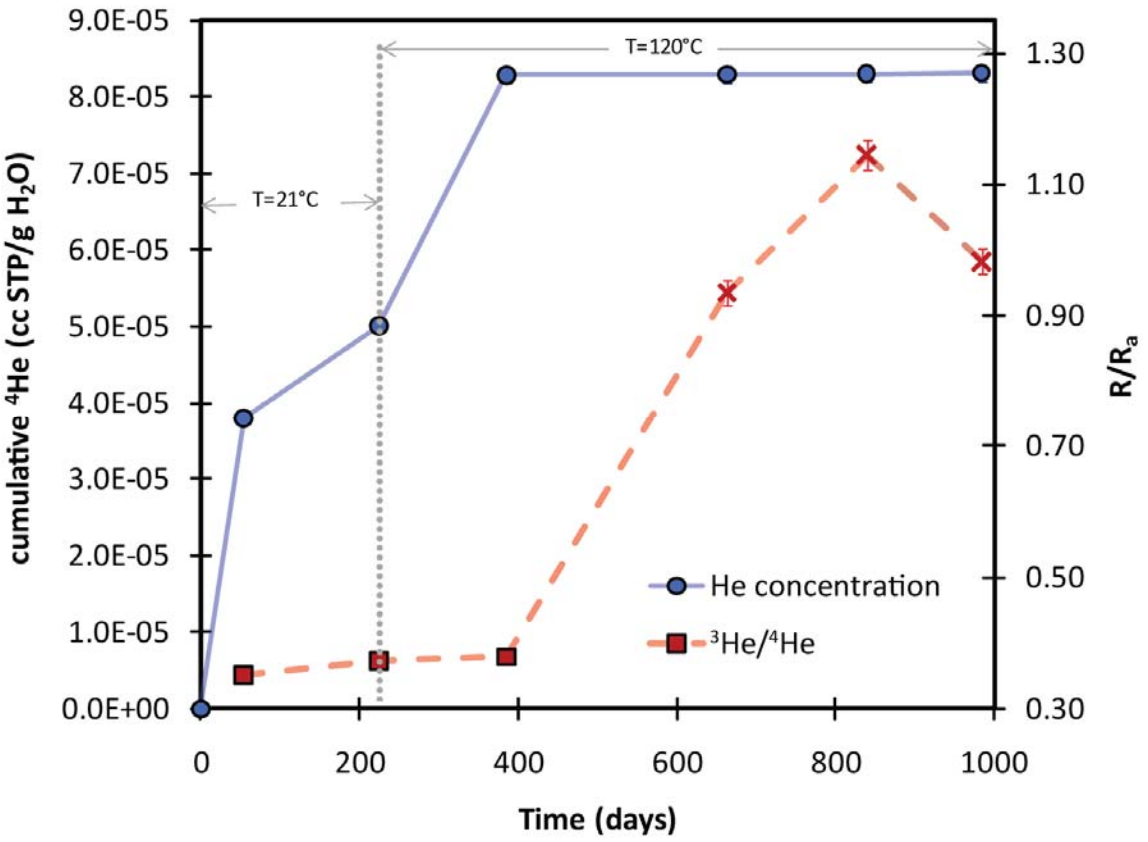

Figure 4: Helium isotope data for SAF 6 (arkosic sandstone, 3064.2-m MD) held at 21°C over two measurements totalling 224 days and then held at 120°C for four measurementrs totaling 775 days. Blue circles represent cumulative helium concentration in extracted pore water over time, while red squares correspond to ^{3}He/^{4}He isotope ratio corresponding to R/Ra axis on the right. The last three data points show negligible contribution to the cumulative helium concentration. However, the ^{3}He/^{4}He has increased to above 1Ra, which corresponds to less than 3% blank contribution from tiny leaks in the container to individual analyses. The last three measurements combined have ~0.3 % of the total cumulative helium concentration. (The absolute amount of gas in the last three measurements combined is less than $3x10^{-7}$ ccSTPg^{-1}). 1σ error bars are smaller than the size of the symbols.

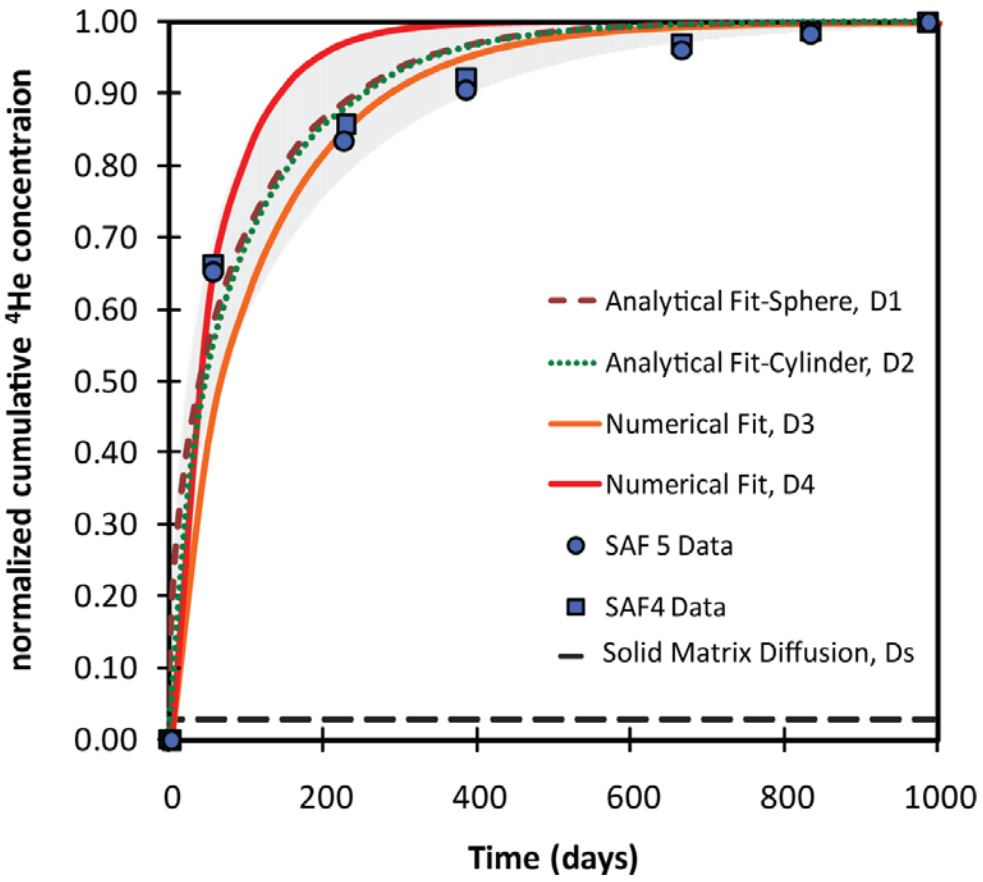

Figure 5: Cumulative helium concentrations normalized to total helium concentration of each sample. Blue markers correspond to SAF 4 (arkosic sandstone, 3059.3-m MD) and SAF 5 (arkosic sandstone, 3056.3-m MD) where both samples were kept at 21°C over six measurements (1000 days). 1σ error bars are smaller than the size of the symbols. Green dotted line represents the analytical solution bounded by cylindrical geometry with a diffusion coefficient of $D_{cylinder} = 1.5x10^{-8}$ cm^2s^{-1}. Red dashed line represents the analytical solution bounded by spherical geometry corresponding to diffusion coefficient of $D_{sphere} = 3.5x10^{-8}$ cm^2s^{-1} ($\pm 1.3x10^{-8}$ cm^2s^{-1}, grey shaded region). Numerical fits for $D_3 = 3.0x10^{-8}$ cm^2s-1 (solid orange curve, $\pm 1.0x10^{-8}$ cm^2s^{-1}) and $D_4 = 6.0x10^{-8}$ cm^2s^{-1} (solid red curve, $\pm 2.0x10^{-8}$ cm^2s^{-1}) superimposed on data and analytical solutions as described in Figure 5. Black dashed line corresponds to theoretical diffusion with $Ds=1x10^{-15}$ cm^2s^{-1} (Solomon et al. 1996) corresponding to diffusion of helium from solid rock matrix.

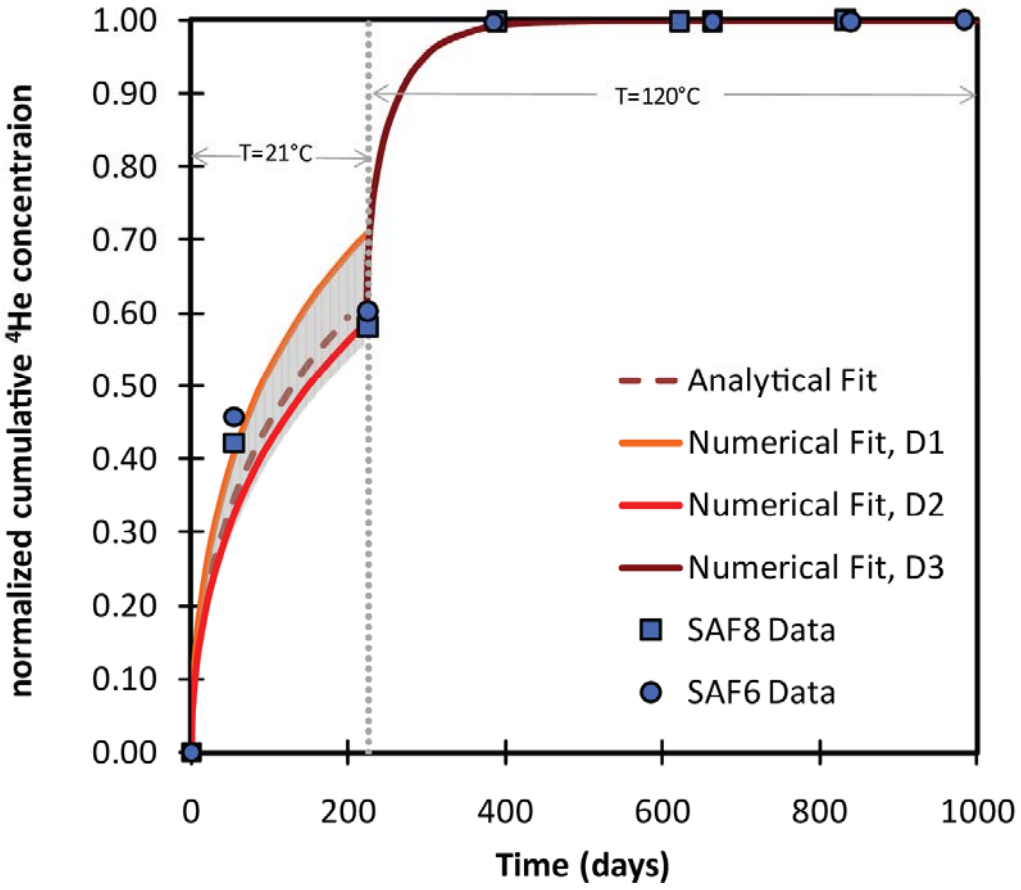

Figure 6: Blue markers correspond to cumulative, normalized helium concentrations for samples-SAF6 (arkosic sandstone, 3064.2-m MD) and SAF8 (arkosic sandstone, 3054.4-m MD) both kept at 21°C over two measurements for 224 days and then kept at 120°C over four to five measurement for 775 days. Red dashed line is the analytical solution bounded by spherical geometry corresponding to diffusion coefficient of D(21°C) = 1.1×10^{-8} cm^2s^{-1} ($\pm 0.4 \times 10^{-8}$ cm^2s^{-1}, grey shaded region). Numerical fits of $D_1(21°C) = 2.5 \times 10^{-8}$ cm^2s^{-1} (solid orange curve), $D_2(21°C) = 1.5 \times 10^{-8}$ cm^2s^{-1} are superimposed on data and analytical solutions as described by $D_3(120°C) = 1.5 \times 10^{-7}$ cm^2s^{-1} (solid brown curve).

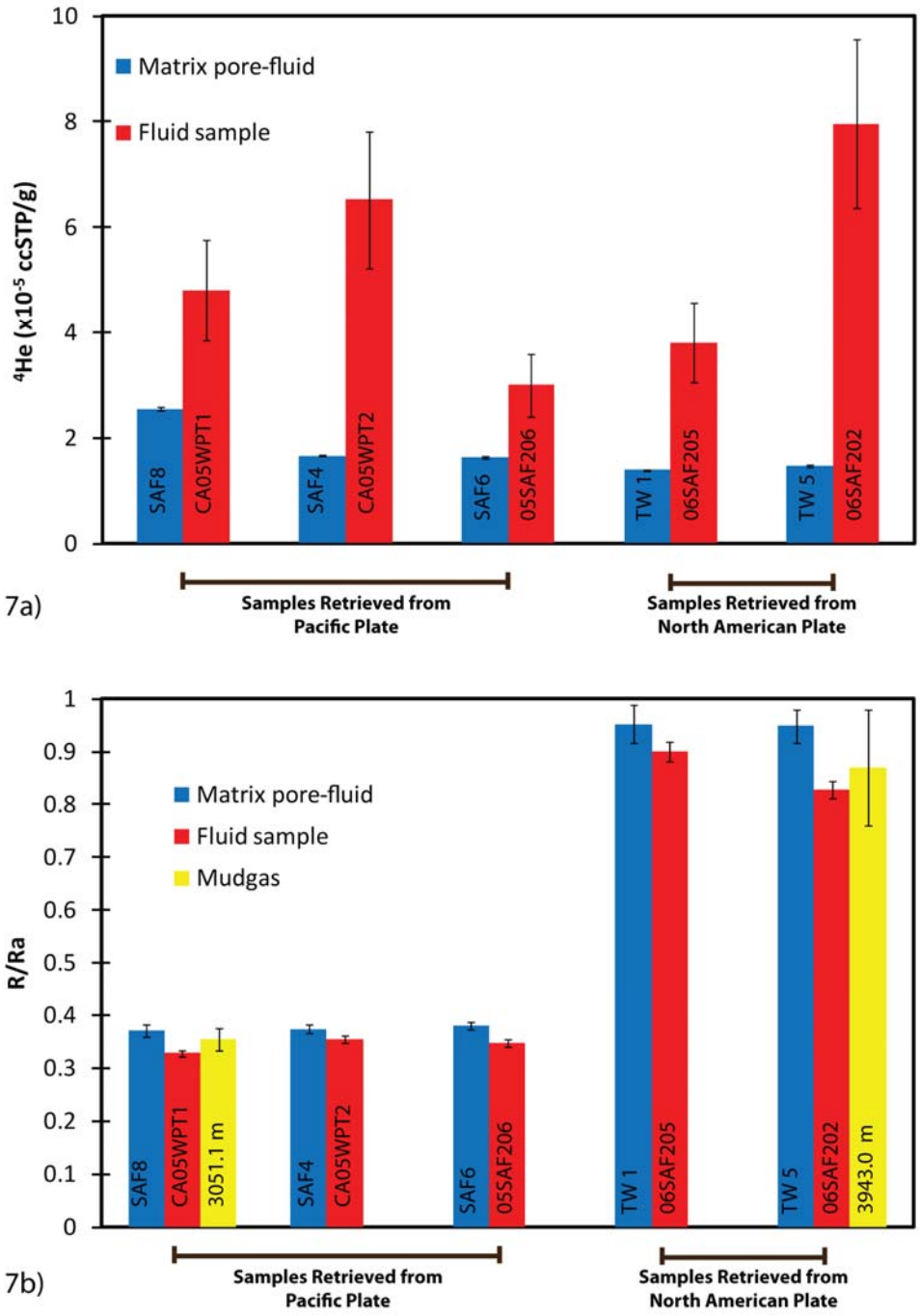

Figure 7: (a) (top panel) Direct fluid sample helium concentrations (red bars, this study) compared to matrix pore fluid samples (blue bars, this study) from similar depths.
(b) (bottom panel) He isotopic ratios (vertical axis, R normalized to air) obtained from three different sample types from nearby locations. Blue bars represent fluid data (this study), red bars correspond to pore fluid data (this study), and yellow bars are based on mudgas data from Wiersberg et al. Two distinct and reproducible isotopic signals are present in the Pacific Plate versus the North American Plate separated by the San Andreas Fault.

Sample ID	Sample Depth (MD, m)	^{4}He [x10^{-5} ccSTPg^{-1}]	(1σ, s.d.)	R/Ra	(1σ, s.d.)	Air ^{4}He contribution (%)	^{20}Ne [x10^{-7} ccSTPg^{-1}]	(1σ, s.d.)	Source
SAF 8	3054.4	2.55	0.03	0.370	0.012	0.11	3.28	0.07	
SAF 5	3056.3	1.67	0.02	0.374	0.008	0.14	5.91	0.12	
SAF 4	3059.3	1.64	0.02	0.380	0.007	0.00	2.51	0.05	
SAF 6	3064.2	1.68	0.02	0.366	0.014	0.60	3.24	0.06	
Mean		*1.88*	*0.44*	*0.373*	*0.006*		*3.73*	*1.50*	1
TW 3	3986.8	1.37	0.02	0.936	0.034	0.45	0.59[T]	0.01	
TW 5	3987.6	1.22	0.02	0.942	0.031	0.61	1.96	0.04	
TW 1	3989.0	1.39	0.02	0.952	0.037	0.00	2.80	0.06	
TW 4	3989.6	1.47	0.02	0.948	0.031	2.91	0.71[T]	0.01	
Mean		*1.36*	*0.10*	*0.945*	*0.007*		*1.51*	*1.06*	
	3051.0			0.354	0.021				2
	3943.0			0.870	0.110				
CA05WPT1	3051.1	4.80	0.10	0.328	0.157				
CA05WPT2	3056.2	6.52	0.13	0.354	0.155				
05SAF206	3064.8	3.00	0.06	0.347	0.157				
Mean		*4.77*	*1.76*	*0.343*	*0.014*		N/A		3
06SAF205	3261.4	3.81	0.08	0.900	0.024				
06SAF202	3726.2	7.96	0.16	0.828	0.025				
Mean		*5.89*	*0.06*	*0.864*	*0.051*				

Table 1: Sample recovery depths (measured depths, M.D.) along borehole. Helium and neon abundance and helium isotope ratios (normalized to air) of pore fluids obtained from diffusion (Source 1: this study), mud-gas samples (Source 2: Wiersberg et al.) released during drilling and well samples (Source 3: measured at LBNL, this study) all obtained from SAFOD drill holes. 3: fluid samples accumulated in borehole in between drilling, R/Ra values measured at LBNL and [He] calculated based on F(4He) and F(40Ar) values and Ar concentrations (Thordsen et al. 2005). [T]Some degassing may have occurred in these samples.

Table 2: Density and porosity values of drill subcore samples used in this study compared to geophysical data from the same depths (MD, m). $Porosity_1$ is based the mass of water extracted during noble gas measurements and subsequent sample drying at 120ºC. $Porosity_2$ is based on mass of water used to re-saturate hand sample after complete extraction of noble gases and drying. % water loss refers to the amount of water lost during experimental pumping and flushing with high purity N2 after each individual sample was re-saturated with degassed DI water. Neutron density and neutron porosity data are from geophysical logs (available from International Continental Scientific Drilling Program--DOI: 10.1594/GFZ.SDDB.1126-1128). # Field normalized compensated neutron porosity.

		Hand sample				Geophysical Log	
Sample ID	**Sample Depth(m)**	**Density (gmL^{-1})**	**$Porosity_1$ (%)**	**H_2O loss (%)**	**$Porosity_2$ (%)**	**Neutron Density (gmL^{-1})**	**Neutron Porosity# (%)**
SAF 8	3054.4	2.5	3.0	2.6	5.8	1.6	5.9
SAF 5	3056.3	2.0	2.3	4.2	5.3	2.1	5.9
SAF 4	3059.3	1.9	2.6	4.6	6.2	1.5	7.7
SAF 6	3064.2	2.0	3.3	3.6	8.9	2.2	19.4
TW 3	3986.8	2.3	4.2	9.0	8.9	N/A	N/A
TW 5	3987.6	2.0	2.2	7.5	2.5	N/A	N/A
TW 1	3989.0	2.3	3.1	6.0	7.2	N/A	N/A
TW 4	3989.6	1.8	2.9	4.0	4.5	N/A	N/A